Effects of sample bias on adhesion of magnetron sputtered Cr coatings on SiC

P.A. Mouche[a,1], A. Evans[b], W. Zhong[a], T. Koyanagi[a], Y. Katoh[a]

[a] *Oak Ridge National Laboratory, Materials Science and Technology Division, Oak Ridge, Tennessee*
[b] *Surface Engineering Group, Manchester Metropolitan University*

Abstract

Swelling of SiC at 300°C due to in-service neutron irradiation causes tensile residual stresses in coatings which are expected to adversely affect the performance of coated SiC composite fuel cladding for light water reactors. Matching the coating swelling with the substrate, a solution common for thermal expansion, is not practical in the case of neutron irradiation. Biasing samples during magnetron sputtering deposition induces compressive residual stress which may counteract this. In this study, chromium coatings were deposited on SiC by DC magnetron sputtering with no external heating at bias voltages of -50V, -75V, and -100V. The effects of the bias voltage on morphology, residual stress, microstrain, texture, and adhesion are shown. The low deposition temperature resulted in the coating microstructure evolution following an energetic particle bombardment dominated trend. At the two lower bias voltages knock-on implantation dominated increasing the residual stress and microstrain while at the highest bias voltage, thermal spike migration allowed for defect relaxation. When the knock-on induced compressive residual stress exceeded 0.8 GPa microcrack formation in the SiC substrate decreased coating adhesion. While no microcracks formed at the lowest bias voltage, insufficient atomic mobility during coating growth lead to voids forming in the coating. A balance is needed to form void-free coatings that have high compressive residual stress.

Keywords: Adhesion, DC magnetron sputtering, Ceramic nuclear fuel cladding, SiC, Residual stress, Texture

[1]Corresponding author
Email address: mouchepa@ornl.gov
mailing address: PO Box 2008, MS6138 Oak Ridge, Tennessee 37831-6138

1. Introduction

Silicon carbide ceramic matrix composites (SiC/SiC) are a possible replacement for traditional zirconium-based fuel rods and core structures in light water reactors [1]. SiC/SiC has better long term radiation stability as well as improved high-temperature capabilities. In the process of developing these composites, hydrothermal corrosion and a loss of hermeticity due to complex neutron irradiation-heat flux-composite structure interactions arose as potential issues [2, 3]. A dual-purpose coating to provide a corrosion barrier and an outer seal is one solution that has garnered interest and attention. Previous research identified Cr as a strong candidate for the coating material due to its corrosion resistance and the possibility for crack mitigation [4, 5, 6, 7, 8, 9, 10]. Chromium is also one of the lead candidate materials for coatings on zirconium-based alloys for nuclear fuel cladding with significant research published on the topic [1, 11, 12, 13, 14]. This work can be leveraged to understand the parameters to make a dense coating that performs well during corrosion, as both SiC and Cr have the same requirements.

The nuclear reactor environment brings a design space that is significantly different than what previous protective coatings on SiC have been designed for. The coatings thickness and material are limited by neutronics, but it will be exposed to a hydrothermal corrosive environment where a thicker coating would be beneficial. Mechanical stresses will form at the interface from the neutron irradiation swelling of the SiC substrate [15] while radiation-induced mechanical degradation of the coating material itself is anticipated. Therefore, a deeper understanding of the possible properties of Cr coatings and interfacial adherence is necessary so that they can be tailored to the needs of a nuclear reactor environment. Physical vapor deposition (PVD) offers a wide array of coating growth methods which can result in dense, high purity coatings. The mechanical and morphological properties of the coatings are highly dependent on the method and deposition parameters, which can be changed to suit the specific application need. Magnetron sputtering is a useful deposition technique gaining a more fundamental understanding of how some of the deposition parameters affect coating performance.

When depositing coatings with magnetron sputtering, increasing the sample bias serves to accelerate the charged ion species in the plasma towards the sample, increasing their kinetic energy. This has a strong effect on the coating growth, particularly on the residual stress [16], with an initial increase in residual stress at lower energies before an inflection point with decrease at higher energies. The inflection point is due to a competition between knock-on based damage from bombardment and annealing due to energy deposition. Controlling stress is of interest as a way to offset the neutron irradiation swelling of the substrate. While it is unknown how much compressive stress can be accommodated before adhesion is affected, initial tests showed that coatings with a

higher initial compressive residual stress were less likely to crack during irradiation [10]. The increased ion energy also benefits coating density due to knock-on effects implanting surface atoms deeper into the coating [17].

There is a substantial body of research on the growth of PVD chromium coatings, with a strong emphasis on the texture. The texture of the coating normal to the surface, whether (110) or (200) planes are preferred can provide insight into the growth conditions of Cr coatings. Understanding the conditions that cause texture changes can help translate the results found here to other PVD methods such as HiPIMS or ion-assisted PVD. Substrate temperature, ion velocity, deposition rate, and impurities all affect the growth conditions of coatings. It appears that the substrate does not have an effect on the texture [18]. There has been significant work in understanding how the different deposition parameters influence the texture of Cr coatings, although with some disagreement. There is a consensus that increasing the substrate temperature promotes the growth of a [200] texture [19, 20, 21, 18], however, Gautier [20] proposed that it was due to impurities rather than a minimizing of surface energy or an increase in mobility. When a bias voltage was introduced at these elevated temperatures the preference changed to a [110] direction. Gautier concluded that increasing the bias voltage sputtered impurities away allowing for [110] texture growth [20]. Feng's [19] explanation was that the increased bombardment at higher bias voltages allowed for the nucleation of [110] direction texture.

The objective of this work is to determine the effects of increased ion energy, as a result of sample bias, on the adhesion of Cr coatings on β chemical vapor deposited (CVD) SiC. Increasing sample bias can lead to an increase in the compressive residual stress; however, the upper limit where coatings will remain adherent is not known. Starting with a significant compressive residual stress is of interest as a route to compensate for the radiation induced swelling of the SiC early in the reactor life which imparts a tensile stress in the coating. Cr coatings have a lower threshold for spalling when stresses are tensile [4]. Matching of swelling, as is practiced with thermal expansion with high temperature coating, is not as feasible with neutron irradiation based swelling due to limitations in elements and fundamentally how radiation induced swelling occurs in materials. Analysis and discussion focus on understanding the changes in the microstructure and the link between the measured residual stresses, coating microstructure, and damage to the SiC to the adhesion of the coating. Due to an unexpected change in the texture, the specifics of the deposition conditions will be addressed in relation to preferred orientation. This serves to inform how sample biasing can be used when designing Cr coatings for use in nuclear reactor environments.

2. Experimental Methods

2.1. Materials

DC magnetron sputter coatings were deposited on flat high resistivity CVD β-SiC coupons obtained from Rohm and Haas (now Dow Chemical Co.). Sample

coupons were machined to 10 x 20 x1 mm with a 2.1 mm hole drilled near the top of the coupon to allow it to be suspended. The sample surface was left in the as-machined state with the typical surface features shown in Fig. 3. Preliminary work found that highly polished surfaces decreased adhesion, and the grinding process used for machining results in peak-to-valley features less than 2μm. This finish is closer to what would be easily achievable for SiC rods. Sample surfaces were observed to be uniform due to the machining process. Coatings were deposited at Manchester Metropolitan University in a DC magnetron sputter coating system. The system consisted of two 300mm by 100mm top-mounted rectangular magnetron deposition heads with Cr targets (bonded to a copper backing plate) of 99.5% purity. Samples rested on a rotating sample holder 10cm below that was biased. Prior to deposition, the chamber was pumped down to a base pressure less than 1 x 10^{-3} Pa. When the base pressure had been reached, inert argon gas was introduced into the system. Three different sample sets were fabricated with samples biased at -50, -75, and -100V with a deposition time of 4 hours each. Coatings were deposited on one side of the coupons, then the coupons were flipped over, and a coating was deposited on the other side. The stage was not heated so any substrate heating came from the energetic atoms. Substrate temperatures were not actively monitored, however, Cr coatings deposited by pulsed DC onto unheated substrates in a similar configuration at a much higher deposition rate measured a substrate temperature of $\sim$100°C [22]. It is expected that increasing the substrate bias will cause a small increase in temperature. Samples were marked to delineate sides.

2.2. Characterization Techniques

Coupled 2θ-θ XRD spectra of the as-deposited coatings were taken using a Bruker D2Phaser diffractometer with a CuK$_\alpha$ ($\lambda = 1.5406A$) source and a LynxEye detector to measure texture. Peak width analysis was performed using the Williamson-Hall (W-H) method [23]. A NIST 640D[24] powder reference was run with a 0.04° step size and a 328s dwell time per step and fit to obtain the instrumental broadening β_i using a pseudo-Voigt peak shape. This was subtracted from the measured broadening β_m of the coatings to obtain their broadening β_c with the following equation,

$$\beta_c^2 = \beta_m^2 - \beta_i^2 \tag{1}$$

The coatings' peak broadening was then plotted with the following equation to obtain the crystallite microstrain ϵ and crystallite size D,

$$\beta_{hkl} cos(\theta) = \frac{k\lambda}{D} + 4\epsilon tan\theta \tag{2}$$

where λ is the x-ray wavelength and k is a shape factor taken to be 0.9. When a line is fit, the crystallite size can be extracted from the intercept and the microstrain can be extracted from the slope.

$\sin^2(\psi)$ residual stress measurements of the coatings were made on a Scintag PTS goniometer with a CuK$_\alpha$ ($\lambda = 1.5406A$) source, a liquid nitrogen cooled Ge detector, and a radial divergence limiting parallel plate collimator. The (310) reflection was used to measure the stress induced Cr peak shift when the sample was tilted from ψ=-55°-55°. These scans were performed at ϕ= 0° and 90° to confirm stress uniformity. DIFFRAC.SUITE EVA was used to strip the Cu Kα_2 peaks before fitting in Origin using a Voigt model. Equation 3 was used to calculate the in-plane coating stress, with the 0° ψ angle peak location serving as the d_0 [25].

$$\sigma = \frac{E}{1+\nu}\frac{1}{d_0}\left(\frac{\partial d_\psi}{\partial sin^2\psi}\right) \tag{3}$$

To examine larger defects in the coatings cross-sectional scanning electron microscopy (SEM) imaging was performed with a Tescan MIRA3 GMH field emission gun-SEM. Cross-sections were fabricated using a low-speed diamond saw to section the coupons, mounting the cut face in epoxy, and mechanically polishing to 0.5um. SEM images were taken in both secondary electron (SE) and back-scatter electron (BSE) modes with a thin carbon coating applied to limit charge buildup.

Transmission Electron Microscopy (TEM) was performed on a JEOL 2100F TEM equipped with a 200 keV Schottky field emission gun to investigate the grain structure and defects of Cr coating. This TEM can operate in scanning mode with the bright-field and high angle annular dark-field (HAADF) imaging capability. TEM samples were prepared using the Focused Ion beam (FEI Quanta 3D 200i and FEI Versa 3D). Standard TEM sample procedure was followed with an initial electron beam deposited layer of Pt to protect the material surface and a final cleaning using 2kV Ga ions to limit damage accumulation.

Pull-off adhesion tests were performed using a DFD instruments PAThandyTM 1kN microadhesion tester and 2.8mm stubs. Testing stubs were mechanically abraded with 320 grit SiC paper to increase surface area and then both stubs and coupons were cleaned with methanol. A single part high strength epoxy (E1100S) was used to bond the stubs to the coatings. Samples were attached to alumina backing disks using the same epoxy to prevent sample fracture during testing. The epoxy was cured at 150°C for 3-4 hours before testing. Tests on as-received coupons showed an epoxy adhesion failure at 85-100 MPa.

3. Results

3.1. Microscopy

STEM bright-field images of the coating cross-sections in Fig. 1 found that the coatings were close to 5μm thick with exact measurements of -50V = 5.6μm, -75V = 5.1μm, and -100V = 4.6μm. A typical columnar structure was observed, with much smaller grains at the interface where nucleation occurred, transitioning to a more uniform grain structure. Grain sizes were sampled in the top two-thirds of the coating by directly measuring the lengths and widths of all the

grains in the fib lift-out (on average 30 grains were measured). Both bright-field (shown) and high-angle annular dark-field (HAADF) image modes were compared to increase the confidence in determining grain boundaries. Measuring both the length and width was done due to the large aspect ratio. Neighboring grains with low angle grain boundaries may be considered as one grain due to the potentially low/no contrast on the grain boundaries. The results of these measurements were put into violin plots and are shown in Fig. 2 with a slight increase in the grain widths and lengths at the -100V bias voltage. The contours in the plots show the distribution of the lengths and widths. All of the samples shared the same range of grain sizes, but the -100V sample had a higher frequency of larger grains.

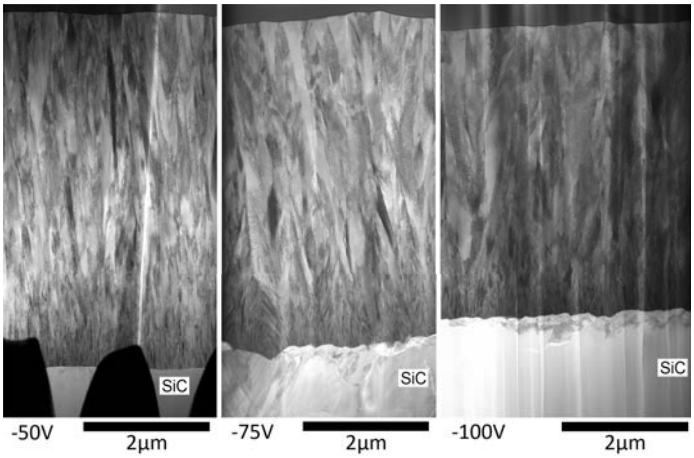

Figure 1: STEM bright-field images of cross sections of Cr coatings on SiC deposited with -50V, -75V, and -100V sample biases.

Not highlighted in the STEM images are the larger coating defects that were present in the -50 and -75V samples. Typical examples of a coating traversing defect and defect density are shown in Fig. 3A and C. Figure 3 B highlights the origin: undulations in the substrate caused columnar grains to nucleate at angles which eventually collided but do not merge. At the lower bias voltage these growth differences could not be overcome, resulting in a continuous crack or void from the substrate to the surface. In the -100V sample the continuous growth of the defects was limited, terminating near the SiC substrate. This is consistent with an increase in the energy of impinging ions [17, 26]

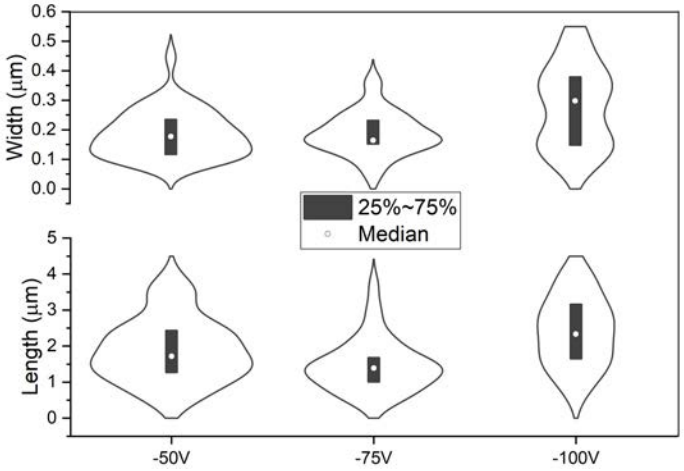

Figure 2: Violin plots showing grain size distributions for the grains taken from the columnar region starting 1um above the interface to the top of the coating. Measurements taken from STEM bright-field and HAADF (not shown) images. Width is parallel to Cr/SiC interface and length is perpendicular. Contours show the relative probability of each grain size.

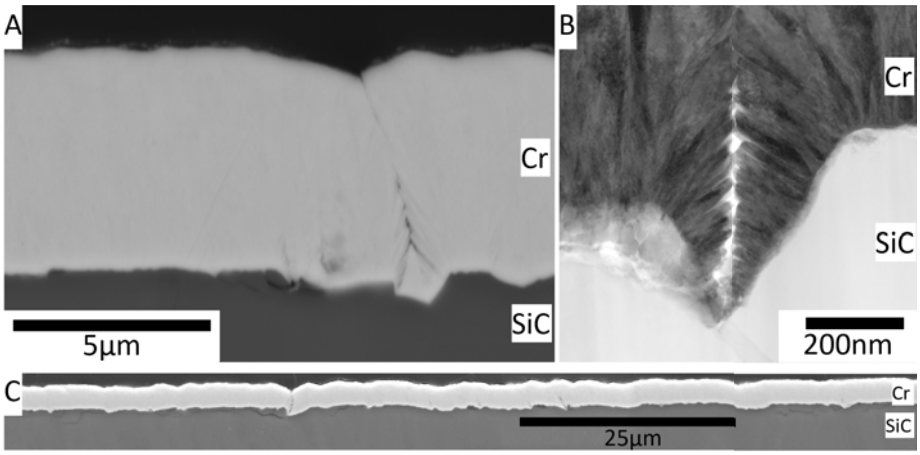

Figure 3: Defects observed in coating cross sections. A) SEM BSE of columnar growth induced defect in -50V sample. B) STEM bright-field of columnar growth defect localized to Cr/SiC interface in -100V sample. C) Representative density of columnar growth defect in -75V sample.

3.2. X-ray analysis

2θ-θ diffraction spectrums (Fig. 4) of the coatings show two major differences between the three bias voltages: a change in the preferred orientation and a change in the full width half maximum (FWHM) of the peaks. By increasing the bias voltage, a shift in the preferred orientation of the grains occurred from [110] to [200]. The FWHM, particularly the (200) and (310) peaks increase from -50V to -75V, and then decrease at -100V. This peak parameter is tied to crystallite size and crystallite microstrain, with a decrease in the size or an increase in microstrain increasing the peak width. Fitting the peak widths with the W-H method results in microstrains listed in Table 1 with the fitted data points shown in Fig. 5 A. Only microstrain values are listed as the intercepts were too close to zero or negative. This was primarily because most of the peak broadening was due to intrinsic microstrain making size effects smaller than the error. This was further validated when the -50V sample with whole pattern Reitveld refinement using GSAS II found a large crystallite size as well as a large microstrain. Since the intercept in W-H analysis trends towards zero the larger the grain size is and since some of the intercepts fit to be negative (which is non-physical), the intercept was set to zero and only the slopes were allowed to vary. The differences in the fits when the intercept is fixed and unfixed are shown in Fig. 5 A.

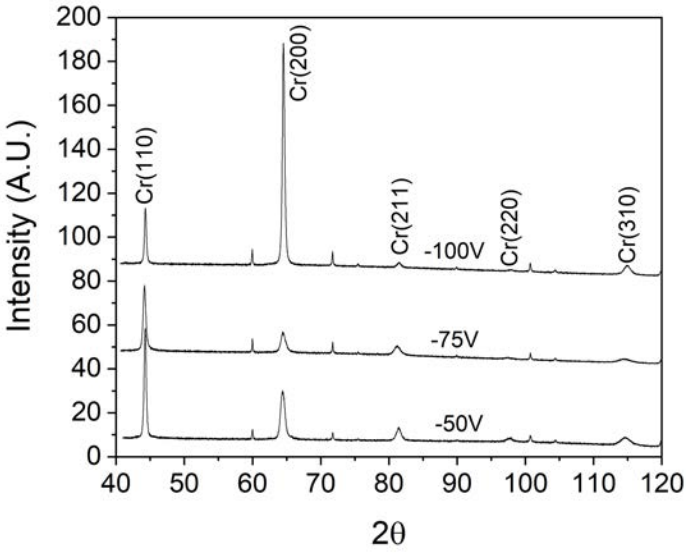

Figure 4: XRD spectrum of as-deposited Cr coatings with small peaks from the underlying SiC. Unlabelled peaks belong to SiC. A transition to the (200) plane can be seen at -100V, along with a decrease in the FWHM.

The results of the residual stress measurements are shown in Table 1 with the fits shown in Fig. 5 B, C, and D. No substantial splitting of the plus and minus ψ directions was observed, both the 0 and 90° sample orientations gave similar

stresses, however some deviation from non-linearity evolved with increasing bias voltage. This was particularly apparent in the -100V sample. This non-linearity is attributed to a gradient in the residual stress. As ψ is tilted, the x-ray path length and penetration depth change. Therefore, the higher ψ angles are more representative of the surface. Since the residual stresses in relation to the pull-off adhesion strength are of interest, only the lower three data points were fit in the -100V sample. The calculated residual stress of the coating would be lower if the last data point was included as well.

Table 1: Residual stress calculated using $sin^2(\psi)$ method and intrinsic crystallite microstrain calculated with the Williamson-Hall method. E = 290GPa $\nu = 0.2$. Negative residual stress values indicate a compressive stress. Williamson-Hall fit with intercept fixed to 0.

Sample Bias	W-H microstrain (ϵ*10-3)	Residual Stress (GPa)
-50V	4.7±0.3	-0.83±0.06
-75V	5.6±0.1	-1.28±0.19
-100V	3.2±0.2	-0.87±0.12

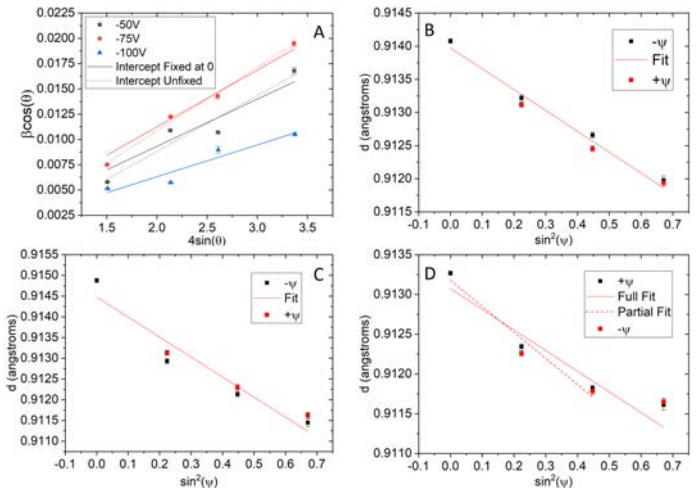

Figure 5: A) fits from Williamson-Hall crystallite size and microstrain analysis. Intercepts were locked at 0 to prevent negative values do to the large intrinsic microstrain values and apparent large crystallite size. B),C),D) fits from $sin^2(\psi)$ residual stress analysis on -50V, -75V, and -100V samples. Deviation from linear indicates a stress gradient.

3.3. Adhesion testing

Pull-off adhesion tests were performed up to three times per sample on multiple samples. The results can be categorized into total delamination, partial delamination, and epoxy failure. The results in Fig. 6 show that the -50V sample never had a coating failure up to 95MPa, the -75V sample was able

to withstand up to the same pressures, but did have a mix of complete and partial delaminations. It should be noted that all the complete delaminations came from the same sample. It was observed that some of the -75V samples showed small amounts of blistering and delamination on several of the coupons that were fabricated. These were not seen in the other bias voltages. Finally, the -100V sample had some partial delamination, but overall was more adherent than the -75V sample.

Looking at both the SiC substrate where Cr was removed, and the bottom of the Cr coating that was bonded to the SiC in Fig. 7 it can be seen that varying amounts of SiC and Cr remained bonded to each other. Therefore, the failure at the interface was both adhesive between the Cr and SiC, but also cohesive in the SiC and Cr near the interface. ImageJ [27] was used to calculate the % area of SiC and Cr that cohesively failed and remained bonded to the Cr and SiC respectively. This analysis was done on a -75V sample with complete delamination, and -75V and -100V samples with partial delamination. Results listed in Table 2 show that while the partial delamination samples had similar amounts of SiC still bonded to the Cr, the sample with complete delamination had a significantly larger fraction of SiC removed. Additionally, the -100V sample had slightly more Cr remaining adherent to the SiC than the -75V samples.

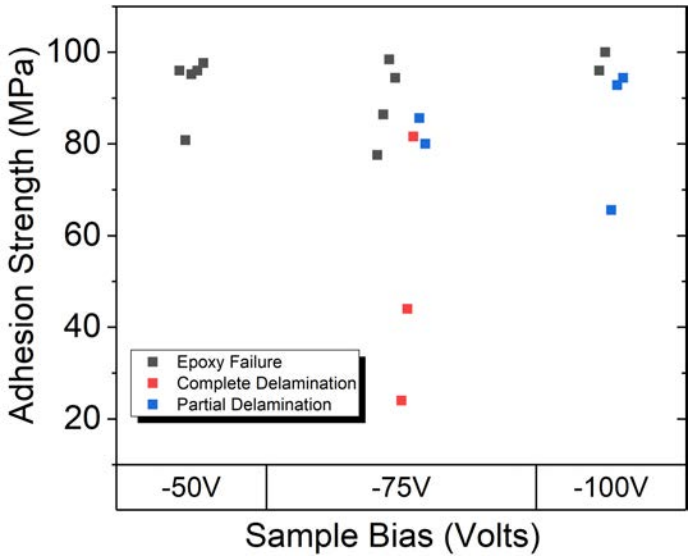

Figure 6: Results of pull-off adhesion testing of the -50V, -75V, and -100V sample biased coatings. The high residual stress in the -75V sample led to early failure in several samples.

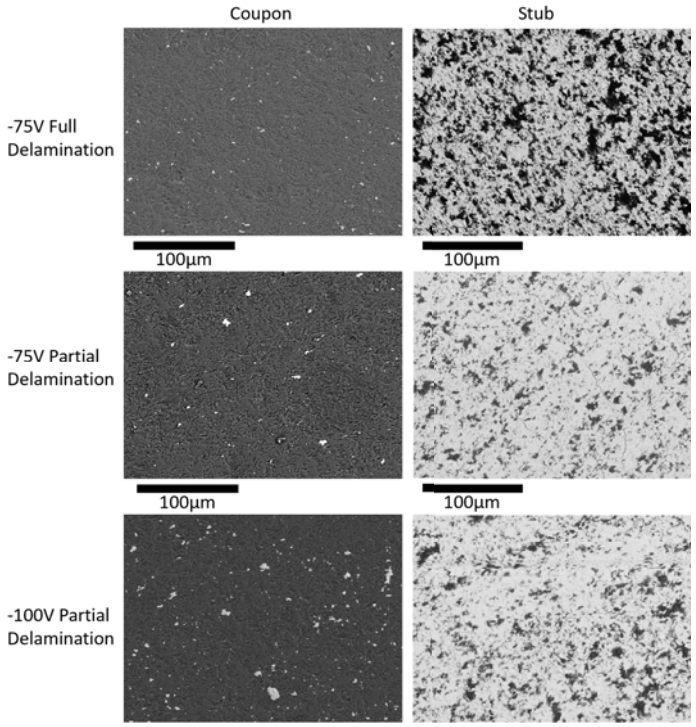

Figure 7: SEM back-scatter images of the coupon and stub post pull-off adhesion testing. SiC appears dark while Cr appears light. Coupon images show the region where the Cr coating was removed, and stub images show the underside of the Cr coating that was pulled away.

Table 2: Fractions of Cr that remained bonded to SiC, and fractions of SiC that remained bonded to the underside of the Cr coating after pull-off adhesion test.

Sample Condition	% area SiC bonded to Cr	% area Cr bonded to SiC	Pull-off stress (MPa)
-75V Complete Delamination	49±3	0.8±0.1	44
-75V Partial Delamination	23±1	0.7±0.1	80
-100V Partial Delamination	29±1	2.6±0.1	94.4

Focusing on the SiC near the Cr/SiC interface in the STEM microscopy (Fig. 8) explains some of the pull-off adhesion test results. Microcracking was observed in the SiC particularly in the -75V and -100V samples. This sampling is limited in area but does point to an additional phenomenon that is important to coating adhesion: coating stress damage to the SiC.

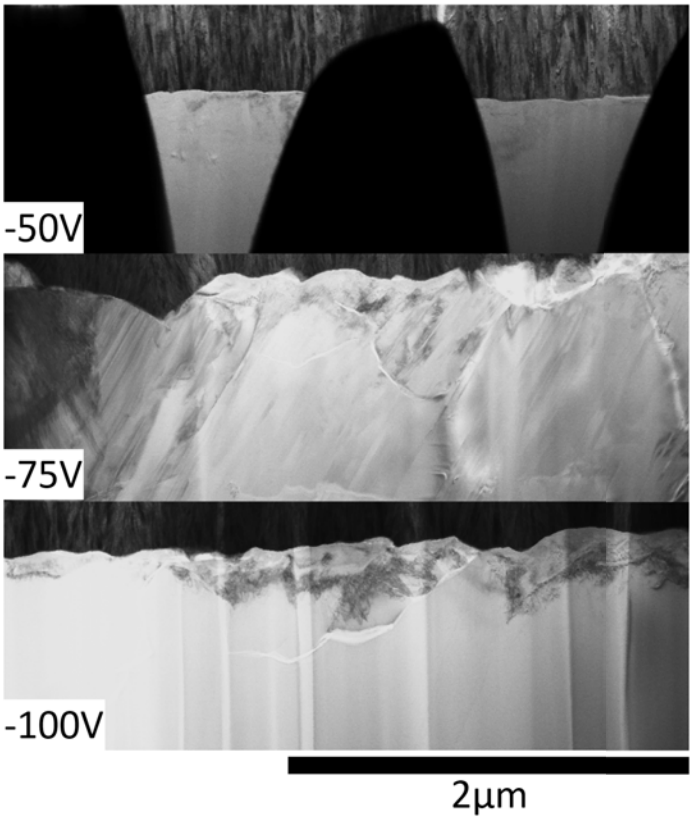

Figure 8: STEM bright-field cross-section images of SiC near the coating interface. Clear microcracks can be seen in the -75V, and -100V biased samples.

4. Discussion

There is an observed dependency of many of the coating properties on the substrate bias. First, the effects and driving mechanisms behind the differences in the coatings will be compared with expected results from previous studies to explain the unexpected texture at -100V. Next, the origin of the adhesion strength as it relates to the observed coating microstructure will be reviewed. Finally, how bias voltage can be used to improve Cr coatings on SiC for use in nuclear reactors will be discussed.

4.1. Mechanism driving coating morphology

The relationship between preferred orientation and substrate bias in the -100V sample does not agree with the Cr coating studies published by Feng and Gautier [19, 20]. These are discussed further in the introduction. In the coatings deposited here, the (200) peak is weak at -50 to -75V and strong at -100V. While heating of the substrate due to deposition is expected [28] and can induce an

orientation change to [200], Gautier's deposition at 400°C steadily transitioned from [200] to (110) with increasing bias. The decrease in the microstrain and residual stress in the -100V samples in our work indicates increased atomic mobility so several -100V samples were annealed at 300°C, 400°C, and 500°C for time periods similar to the growth time. It was found that the microstrain and residual stress related peak shifts in XRD were not significant until 500°. This temperature is much higher than what would occur without substrate heating, thus the changes observed in the -100V sample were not caused by bulk heating.

Increasing the ion velocity is another method to increase atomic mobility, but its effects are not as straight forward as bulk heating. The changes observed in the residual stress, microstrain, and void formation do agree with an incident ion energy controlled mechanism. From theoretical models of film stress [16], there is expected to be an initial increase in the residual stress as more atoms are implanted into the coating and create damage regions. However, at sufficient ion energies, these can be relaxed by the thermal spikes introduced by the ions leading to a reduction in the residual stress. It can be interpreted that the decrease in the residual stress at -100V was caused by the threshold of incident ion energy being reached. However, there may be additional mechanisms affecting the coating growth, as the necessary ion energy for this is generally fairly high [29]. Determining the exact growth processes is outside of the scope of this work.

The changes in the crystallite microstrain were very similar to the residual stress, most likely due to a dependence of the microstrain on the same defects that lead to compressive residual stress [30, 31]. In coatings, microstrain can form from both the introduction of defects during the ballistic collision, as well as when the residual stress becomes greater than the yield stress causing plastic deformation. Microstrain during yielding usually occurs when the residual stress forms due to the coefficient of thermal expansion (CTE) mismatch when the samples are cooling after coating. Yielding as a source of defects is most likely not the mechanism here as the coatings were deposited at lower temperatures due to the lack of external heating and Cr has a larger CTE than SiC so any residual stress that would arise from cooling would be counter to the compressive stresses observed. Therefore, both the microstrain and residual stress can be assumed to be linked to the same mechanisms.

A sufficiently high ion velocity may also explain the texture. Ion velocities up to 250eV produced from -250V biasing have been observed to shift the texture of Cr coatings to (200) in arc ion plating at 250°C [32] as well as the introduction of Ar^+ ion irradiation during pulsed laser deposition at with no external heating [33]. DC magnetron sputtering has a large density of ionized Ar [34]. It is most likely that a similar phenomenon occurred here causing the change to (200) texture given the agreement between the other coating properties and ion velocity. Comparing with Gautier's work [20], this does point to an interesting relationship between the substrate temperature and the ion velocity effect. A high substrate bias, which is associated with (200) textures at lower temperatures, was required to induce a (110) texture in a substrate which was

at a temperature where a (200) texture would form. Increasing the substrate temperature may work to suppress the ion velocity effect on texture.

Taking the various changes in coating morphology into account it is clear that the coating growth was controlled by ion bombardment. at -50V and -75V the coating is in an ion knock-on dominated state with high levels of defects and poor structure. At -100V thermal spikes may activate sufficient migration to recover from some of this damage and change the crystallographic texture.

4.2. Relationship between adhesion strength and sample bias

The pull-off adhesion tests showed a strong bond between the Cr and the SiC in the -50V sample. This sample showed no partial or complete delamination, withstanding close to 100 MPa of tensile stress normal to the bond plane. The -100V sample results are surprising as it had a slightly higher measured residual stress, but experienced partial delamination. The delamination failure in the -75V sample is not surprising as it had the largest residual stresses nearly 50% larger than the -50V and -100V sample. Some small spots of spalling could be observed with the naked eye on select samples. While several samples were able to stay adherent up to epoxy failure (of 95 MPa), partial and complete delamination was more common. Looking at the microscopy of the failure sites, it is clear that cohesive failure occurred in both the Cr and SiC as well as at the interface. The -75V sample which completely delaminated at low loads had a very high percentage surface covering of SiC removed. The -75V and -100V partial delamination samples had similar bonded areas, but the -100V sample had nearly 3 times the amount of Cr that remained bonded to the SiC. It would be expected that the increased displacement from the higher ion velocity at increased bias voltages [35] would increase adhesion. It is unlikely that this would be coupled with excessive damage to the SiC substrate which could lead to cracking. A quick SRIM calculation [36] shows that Cr ions with energies of 250eV, well above what is expected for the experimental parameters, have a penetration depth of 12 angstroms. The deposition rate would quickly cover and protect the substrate in several seconds with damage limited to the very near surface.

The substantial microcracking in the -75V samples and scattered microcracking in the -100V samples observed with TEM would localize the stress to uncracked regions that could transmit loads in the SiC bulk. Therefore, even if there is increased adhesion between SiC and Cr, this can be nullified by cohesive failure. This is the most likely cause for the partial delamination in the -100V sample. Given the similar residual stresses between -50V and -100V but the differences in substrate cracking, the residual stress at -100V may have been larger earlier in the deposition process. The non-linearity of the $sin^2(\psi)$ in Fig. 5 D shows a gradient in the residual stress with greater stress values when the x-rays had greater penetration (lower ψ angles). The increased atomic mobility that has been associated with the changes in the -100V sample might also be responsible for the residual stress gradient.

Given that failure observed in these load ranges is partially dependent on statistical microcracking in the SiC, then the slight residual stress increase be-

tween the -50V and -100V samples might represent a threshold where localized failure is more likely to occur given the sample dimensions. The theoretical fracture strength of SiC is well over 2 GPa when measured in small volumes [37], however, this decreases to 0.4-0.9GPa when larger samples are tested in various ways [38, 39]. The compressive residual stress in the coating ranging from 0.8-0.9 GPa exerts a tensile force on the substrate that is in-line with the fracture strength of select CVD SiC tensile specimens reported by Lee [38]. The failure criteria for coating delamination is different from SiC failure, requiring multiple flaws to form and transfer stress to the bonded regions. The partial delamination in the -100V samples was limited in area reflecting a lower density of these cracks, as compared to -75V where a higher micro-crack density lead to larger partial and complete delamination. Due to the complicated requirements for delamination, a more in-depth analysis testing various stub sizes, residual stress values in the range of 0.8-1 GPa, and microcrack density is necessary to determine a statistical distribution for failure. The adhesion results indicate that a compressive residual stress of 0.8 GPa is an acceptable level of stress to have in a Cr coating on SiC without adversely affecting the adhesion for the given testing area.

4.3. Optimizing coatings

In other work by our group it was observed that tensile stresses above 0.35 GPa led to cracking and delamination of Cr coatings on SiC. Therefore, an acceptable range of residual stress for these coatings can be established between 0.8 GPa of compressive stress and 0.35 GPa of tensile stress. Although the differences in the thermal expansion of SiC and Cr will lead to a slight compressive stress at the 300°C operating temperature, the neutron irradiation-induced swelling of the SiC will lead to a much larger tensile residual stress in the coating. Therefore, a deposition induced compressive residual stress via sample biasing can serve to partially mitigate the eventual substrate swelling. Neutron irradiation studies at the High Flux Isotope Reactor at Oak Ridge National Laboratory are planned to investigate this.

The existence of an intermediate sample bias which leads to a delamination inducing residual stress is problematic. Depositing below that threshold to limit compressive residual stress is not an adequate solution as this introduces large voids into the coating giving it a low density. These could nullify the hermeticity of the coating and would provide attack sites for hydrothermal corrosion. Of the three biases, the -100V sample showed the best result but could be improved. The gradient in the residual stress observed in the -100V sample does provide an interesting opportunity. Starting the deposition with a -50V sample bias to protect the interface, and then switching to a -100V or higher sample bias to terminate initial voids is a potential solution. However, this relies on achieving a consistent ion velocity to activate the atomic mobility necessary for the recovery. The addition of substrate heating may help limit the maximum achievable residual stress.

5. Conclusions

Five μm Cr coatings were deposited with no external heating on CVD SiC by magnetron sputtering with -50V, -75V, and -100V substrate bias voltages. Findings are listed below:

- Coating microstructure followed what would be expected for a high energy atom bombardment dominated mechanism with a transition from knock-on to thermal spike migration regimes. The crystallographic texture present in the thermal spike migration regime is not commonly observed in previous Cr coating work and may be related to the low deposition temperature.
- Delamination failure was driven by stress-induced microcracking in the SiC substrate. Although ballistic mixing can increase the adhesive strength between the Cr and SiC, stress-induced microcracks in the SiC substrate cause cohesive failure in the SiC which dominates the failure mechanism. Compressive residual stresses greater than 0.8 GPa are necessary to cause the SiC microcracking.
- The -100V sample resulted in the best combination of coating density and adhesion. Improvements can be made during the deposition process to fully eliminate the limited substrate cracking that did occur.

6. Acknowledgements

This work was sponsored by the U.S. Department of Energy, Office of Nuclear Energy, Advanced Fuel Campaign of Nuclear Technology Research & Development program under contact DE-AC05-00OR22725 with Oak Ridge National Laboratories managed by UT Battelle, LLC. This research used the resources of the Low Activation Materials Development and Analysis Laboratory, a DOE Office of Science research facility operated by the Oak Ridge National Laboratory. The authors thank John Echols and Tim Lach for their comments.

7. Data availability

The raw/processed data required to reproduce these findings cannot be shared at this time due to technical or time limitations.

References

[1] K. A. Terrani, Accident tolerant fuel cladding development: Promise, status, and challenges, Journal of Nuclear Materials 501 (2018) 13–30.

[2] T. Koyanagi, Y. Katoh, J. George, C. P. Deck, Issue Update to LWR SiC/SiC Cladding Handbook of Properties, Technical Report, Oak Ridge National Lab.(ORNL), Oak Ridge, TN (United States), 2018.

[3] T. Koyanagi, Y. Katoh, G. Singh, C. M. Petrie, C. P. Deck, K. A. Terrani, X-ray computed tomography analysis of neutron-irradiated sic composite tube, Transactions 120 (2019) 354–355.

[4] P. A. Mouche, T. Koyanagi, D. Patel, Y. Katoh, Adhesion, structure, and mechanical properties of cr hipims and cathodic arc deposited coatings on sic, Surface and Coatings Technology 410 (2021) 126939.

[5] P. Mouche, C. Ang, T. Koyanagi, P. Doyle, Y. Katoh, Characterization of pvd cr, crn, and tin coatings on sic, Journal of Nuclear Materials 527 (2019) 151781.

[6] S. S. Raiman, C. Ang, P. Doyle, K. A. Terrani, Hydrothermal corrosion of SiC materials for accident tolerant fuel cladding with and without mitigation coatings, in: J. H. Jackson, D. Paraventi, M. Wright (Eds.), Proceedings of the 18th International Conference on Environmental Degradation of Materials in Nuclear Power Systems – Water Reactors, Springer International Publishing, Cham, 2018, pp. 259–267.

[7] S. Raiman, P. Doyle, C. Ang, Y. Katoh, K. Terrani, Hydrothermal corrosion of coatings on silicon carbide in boiling water reactor conditions, CORROSION 75 (2018) 217–223.

[8] C. Ang, C. Kemery, Y. Katoh, Electroplating chromium on cvd sic and sicf-sic advanced cladding via pyc compatibility coating, Journal of Nuclear Materials 503 (2018) 245–249.

[9] P. J. Doyle, S. S. Raiman, R. Rebak, K. A. Terrani, Characterization of the hydrothermal corrosion behavior of ceramics for accident tolerant fuel cladding, in: Proceedings of the 18th International Conference on Environmental Degradation of Materials in Nuclear Power Systems–Water Reactors, Springer, 2019, pp. 1485–1496.

[10] P. J. Doyle, T. Koyanagi, C. Ang, L. Snead, P. Mouche, Y. Katoh, S. S. Raiman, Evaluation of the effects of neutron irradiation on first-generation corrosion mitigation coatings on sic for accident-tolerant fuel cladding, Journal of Nuclear Materials (2020) 152203.

[11] J.-C. Brachet, I. Idarraga-Trujillo, M. L. Flem, M. L. Saux, V. Vandenberghe, S. Urvoy, E. Rouesne, T. Guilbert, C. Toffolon-Masclet, M. Tupin, C. Phalippou, F. Lomello, F. Schuster, A. Billard, G. Velisa, C. Ducros, F. Sanchette, Early studies on Cr-coated Zircaloy-4 as enhanced accident tolerant nuclear fuel claddings for light water reactors, Journal of Nuclear Materials 517 (2019) 268–285.

[12] J. Krejčí, J. Kabátová, F. Manoch, J. Kočí, L. Cvrček, J. Málek, S. Krum, P. Šutta, P. Bublíková, P. Halodová, et al., Development and testing of multicomponent fuel cladding with enhanced accidental performance, Nuclear Engineering and Technology 52 (2020) 597–609.

[13] W. Xiao, H. Chen, X. Liu, D. Tang, H. Deng, S. Zou, Y. Ren, X. Zhou, M. Lei, Thermal shock resistance of tin-, cr-, and tin/cr-coated zirconium alloy, Journal of Nuclear Materials 526 (2019) 151777.

[14] J. Huang, S. Zou, W. Xiao, C. Yang, D. Tang, H. Yu, L. Zhang, K. Zhang, Influences of arc current on microstructure of cr coating for zr-4 alloy prepared by multi-arc ion plating via ebsd, Materials Characterization (2021) 111211.

[15] Y. Katoh, T. Koyanagi, J. L. McDuffee, L. L. Snead, K. Yueh, Dimensional stability and anisotropy of sic and sic-based composites in transition swelling regime, Journal of Nuclear Materials 499 (2018) 471–479.

[16] C. Davis, A simple model for the formation of compressive stress in thin films by ion bombardment, Thin solid films 226 (1993) 30–34.

[17] K.-H. Müller, Model for ion-assisted thin-film densification, Journal of applied physics 59 (1986) 2803–2807.

[18] R. Miller, H. Holland, Crystallographic orientation of sputtered cr films on glass and glass–ceramic substrates, Thin Solid Films 298 (1997) 182–186.

[19] Y. Feng, D. Laughlin, D. Lambeth, Formation of crystallographic texture in rf sputter-deposited cr thin films, Journal of applied physics 76 (1994) 7311–7316.

[20] C. Gautier, J. Machet, Effects of deposition parameters on the texture of chromium films deposited by vacuum arc evaporation, Thin Solid Films 289 (1996) 34–38.

[21] S. Duan, J. Artman, B. Wong, D. Laughlin, Study of the growth characteristics of sputtered cr thin films, Journal of applied physics 67 (1990) 4913–4915.

[22] D. Sidelev, G. Bleykher, M. Bestetti, V. Krivobokov, A. Vicenzo, S. Franz, M. F. Brunella, A comparative study on the properties of chromium coatings deposited by magnetron sputtering with hot and cooled target, Vacuum 143 (2017) 479–485.

[23] B. Warren, B. Averbach, The separation of cold-work distortion and particle size broadening in x-ray patterns, Journal of applied physics 23 (1952) 497–497.

[24] D. R. Black, D. Windover, A. Henins, D. Gil, J. Filliben, J. P. Cline, Certification of nist standard reference material 640d, Powder Diffraction 25 (2010) 187–190.

[25] B. D. Cullity, Elements of X-ray Diffraction, Addison-Wesley Publishing, 1956.

[26] J. Lin, J. J. Moore, W. D. Sproul, S. L. Lee, J. Wang, Effect of negative substrate bias on the structure and properties of ta coatings deposited using modulated pulse power magnetron sputtering, IEEE transactions on plasma science 38 (2010) 3071–3078.

[27] C. A. Schneider, W. S. Rasband, K. W. Eliceiri, Nih image to imagej: 25 years of image analysis, Nature methods 9 (2012) 671–675.

[28] V. I. Shapovalov, A. E. Komlev, A. S. Bondarenko, P. B. Baykov, V. V. Karzin, Substrate heating and cooling during magnetron sputtering of copper target, Physics Letters A 380 (2016) 882–885.

[29] J. Hsieh, C. Li, W. Wu, R. Hochman, Effects of energetic particle bombardment on residual stress, microstrain and grain size of plasma-assisted pvd cr thin films, Thin Solid Films 424 (2003) 103–106.

[30] D. Rickerby, A. Jones, A. Perry, Structure of titanium nitride coatings deposited by physical vapour deposition: A unified structure model, Surface and Coatings Technology 36 (1988) 631–646.

[31] D. Rickerby, Internal stress and adherence of titanium nitride coatings, Journal of Vacuum Science & Technology A: Vacuum, Surfaces, and Films 4 (1986) 2809–2814.

[32] M. Hu, M. Shen, Z. Liu, C. Guo, Q. Li, S. Zhu, Self-ion bombarded cr films: Crystallographic orientation and oxidation behaviour, Corrosion Science 143 (2018) 212–220.

[33] M. Shima, A. Ford, C. Ross, Crystallographic and magnetic properties of cocrpt/cr films produced by pulsed laser deposition, IEEE transactions on magnetics 36 (2000) 2321–2323.

[34] A. Ferrec, J. Keraudy, S. Jacq, F. Schuster, P.-Y. Jouan, M. Djouadi, Correlation between mass-spectrometer measurements and thin film characteristics using dcms and hipims discharges, Surface and Coatings Technology 250 (2014) 52–56.

[35] J. Sprague, C. Gilmore, Molecular dynamics simulations of film-substrate interface mixing in the energetic deposition of fcc metals, Thin Solid Films 272 (1996) 244–254.

[36] J. F. Ziegler, M. D. Ziegler, J. P. Biersack, Srim–the stopping and range of ions in matter (2010), Nuclear Instruments and Methods in Physics Research Section B: Beam Interactions with Materials and Atoms 268 (2010) 1818–1823.

[37] H. D. Espinosa, B. Peng, N. Moldovan, T. Friedmann, X. Xiao, D. Mancini, O. Auciello, J. Carlisle, C. Zorman, M. Merhegany, Elasticity, strength, and toughness of single crystal silicon carbide, ultrananocrystalline diamond, and hydrogen-free tetrahedral amorphous carbon, Applied physics letters 89 (2006) 073111.

[38] H. M. Lee, K.-I. Park, J.-Y. Park, W.-J. Kim, D. K. Kim, High-temperature fracture strength of a cvd-sic coating layer for triso nuclear fuel particles by a micro-tensile test, Journal of the Korean Ceramic Society 52 (2015) 441.

[39] S.-G. Hong, T.-S. Byun, R. A. Lowden, L. L. Snead, Y. Katoh, Evaluation of the fracture strength for silicon carbide layers in the tri-isotropic-coated fuel particle, Journal of the American Ceramic Society 90 (2007) 184–191.